HHS Public Access

Author manuscript

Nano Lett. Author manuscript; available in PMC 2019 April 26.

Published in final edited form as:

Nano Lett. 2018 September 12; 18(9): 6100–6105. doi:10.1021/acs.nanolett.8b03163.

Cells adhering to 3D nanoscales: Cell membrane reshaping without stable internalization

Michele Dipalot[‡,a], **Allister F. McGuiret**[‡,c], **Hsin-Ya Lou**[c], **Valeria Caprettini**[a,†], **Giovanni Melle**[a], **Giulia Bruno**[a], **Claudia Lubrano**[b], **Laura Matino**[b], **Francesco De Angelis**[a], **Bianxiao Cui**[c], and **Francesca Santoro**[b]

[a]Istituto Italiano di Tecnologia, Genova, Italy

[b]Center for Advanced Biomaterials for Healthcare, Istituto Italiano di Tecnologia, Napoli, Italy

[c]Chemistry Department, Stanford University

Abstract

The dynamic interface between the cellular membrane and three-dimensional nanostructures determines biological processes and guides the design of novel biomedical devices. Despite recent advancements in the fabrication of artificial bio-interfaces have yielded an enhanced understanding of this interface, there remain open questions on how the cellular membrane reacts and behaves in the presence of sharp objects at the nanoscale. Here, we provide a multifaceted characterization of the cellular membrane's mechanical stability when closely interacting with high aspect-ratio three-dimensional vertical nanostructures, providing strong evidence that vertical nanostructures spontaneously penetrate the cellular membrane to form a steady intracellular coupling only in rare cases and in specific conditions. The cell membrane is able to conform tightly over the majority of structures with various shapes while maintaining its integrity.

Graphical Abstract

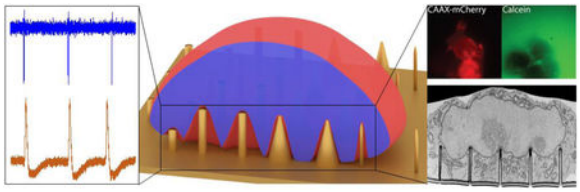

Corresponding Authors: Francesca Santoro, Francesca.santoro@iit.it, , Center for Advanced Biomaterials for Healthcare, Istituto Italiano di Tecnologia, Napoli, Italy. Bianxiao Cui, bcui@stanford.edu, Department of Chemistry, Stanford University. Francesco De Angelis, Francesco.deangelis@iit.it, Istituto Italiano di Tecnologia, Genova, Italy.

[†]**Present Addresses:** V.C. present address: Department of Craniofacial development and Stem Cell Biology, King's College London, SE1 9RT, London, United Kingdom

Author's Contributions

The manuscript was written through contributions of all authors. All authors have given approval to the final version of the manuscript.

[‡]These authors contributed equally.

Supporting Information. The following files are available free of charge. Experimental procedure (PDF), Supplemental figures (PDF).

Notes

The authors declare no competing financial interest.

Keywords

3D nanostructures; cell penetration; electrophysiology; electroporation; cell membrane deformation; cell cross-section; bio-interface

The development of three-dimensional (3D) nanostructures has improved the performance and expanded the capabilities of biosensors used in a variety of biological applications. Drug delivery[1], electrophysiological recording[2], and fluorescence microscopy[3] are the fields in which 3D nanostructures have had the greatest impact. By activating the engulfment machinery of mammalian cells[4], 3D nano-objects improve the coupling between the detector and the cellular membrane[5,6], in some cases yielding access to the intracellular compartment by means of cell membrane poration[7–9].

Various 3D nanostructures have been investigated over the years in the search for the optimal interface for the target application. For example, sharp nanopillars and hollow nanocylinders have been exploited for intracellular drug delivery[1,10,11], and molecular sampling[12], whereas bulk nanopillars and mushroom-like microstructures have been used for intracellular recording of action potentials[7–9,13,14].

Despite these promising successes, the nature of the interface between cells and 3D nano-objects still lacks detail, especially with respect to membrane conformation to nanometer-sharp features[5,6]. More specifically, whether the membrane spontaneously ruptures when cells adhere to sharp nanostructures is debated[15–17]. Furthermore, if it does indeed rupture, the nature of that event (how often and the stability of the rupture), determines the future design of nanostructured devices. A stable rupture that occurs reliably could enable unprecedented measurements of intracellular phenomena. An unstable rupture, in contrast, would lead to reduced control of the device. In the majority of applications for nanostructured devices, control of the interface is desirable. One advantage of control is the possibility to choose when to switch from extracellular to intracellular measurement (i.e. in electrophysiology). A second advantage of control is the ability to precisely deliver to or sample from the intracellular space. To design control into these nanostructured devices, whether they are for diagnosis, genetic manipulation, or treatment, one must be able to measure the integrity of the membrane at the interface between the structure and the cell.

In this work, we employ three independent methods to shed light on how the cell membrane adapts to 3D nanostructures with several different shapes, demonstrating that the cellular membrane can conform to various shapes without spontaneous rupturing. We achieve a comprehensive view of this interface by using fluorescence microscopy to give a biological readout, electrical recording to give a functional readout, and electron microscopy to directly show the physical picture.

The cell penetration experiments were carried out on diverse nanostructured shapes. In particular, we fabricated four different shapes consisting of solid short nanopillars (SSP, h ~ 1 μm, d ~ 200 nm), solid tall nanopillars (STP, h ~ 2 μm, d ~ 200 nm), solid tall nanocones (STC, h ~ 2 μm, d ~ 800 nm), and sharp nanopillars (SP, h ~ 2 μm, d ~ 80 nm). For scanning electron microscopy (SEM) and fluorescence microscopy, cardiomyocyte-like HL-1 and

human embryonic kidney (HEK) cells, respectively, were cultured on these substrates under identical conditions and chemically fixed at different phases. The first phase, named “approaching”, relates to the initial adhesion of cells within the first 4 hours of incubation after plating. The monitoring of the cell/nanostructure interface during the first hours after plating importantly captures the early settlement of cells on 3D nanostructured substrates, possibly revealing relevant dynamic behaviors in the presence of high-aspect-ratio protruding objects. The second phase, named “spreading”, considers the further adhesion and proliferation of cells in the first 24 hours of incubation. Here, we are interested especially in how the cells interact with the 3D nanostructures during cell mitosis and growth.

Fluorescence imaging

Fluorescence imaging has been used to monitor intracellular delivery of a membrane-impermeant fluorophore into cells growing on 3D nanostructures. In these experiments, the solid short pillar structures were made of quartz, and the solid tall pillars and cones made of cross-linked polymer. Delivery of the fluorophore due to possible spontaneous penetration of the nanostructures was measured at 4 h and 24 h after cell plating to correlate with previous experiments presented in literature[1,18,19] which emphasize that cellular adhesion plays a key role in facilitating penetration events[18]. The fluorophore, calcein, is commonly used in studies of endocytosis dynamics due to its cell-impermeant nature and stable fluorescence[20]. Here, CAAX-mCherry-transfected HEK293 cells[21] were plated on the poly-L-lysine-coated nanostructures and imaged after 10 min. incubation with calcein and subsequent washout. Brightfield images were taken to register the pillars, images of CAAX to track the cell membrane, and images of calcein to visualize penetration events (Fig. 1). In order to analyze the presence of penetration events, the pillar area was masked according to brightfield images, and corresponding calcein fluorescence intensity quantified. There are some cases where high calcein intensity is observed in a non-punctuated pattern; this is attributed to calcein binding to cellular debris. In the majority of images (22 of 23), across geometries and at both 4 h and 24 h, calcein was not found to be concentrated interior to the cell membrane. [AFM TO ADD TEXT HERE WITH QUANTIFICATION INCLUDING SHARP PILLARS.] In one case, cell apoptosis (determined by the phenotype of the cell membrane) yielded bright puncta of calcein which is expected when the cell membrane permeabilizes during apoptosis (Fig. S1). Such data suggest that these four geometries--short pillars, tall pillars, tall cones, and sharp pillars--do not reliably spontaneously penetrate HEK293 cells in the tested temporal window.

Electrophysiology

The shape of action potentials recorded with multielectrode arrays (MEA) depends strongly on the integrity of the cellular membrane in contact with the 3D nanostructures. If the membrane is intact, and in absence of special functionalization[22], the typical detected signals are extracellular spikes with a predominant negative potential phase. If the membrane presents pores and the 3D nanostructures are in contact with intracellular compartment, the MEA records intracellular action potentials with a predominant positive potential phase and a completely different shape. Thus, electrophysiological recording can

provide a clear indication of the membrane integrity at the interface with 3D nanostructures. Moreover, electrophysiological recording is performed over time on live cells and allows for a real-time investigation of the membrane integrity during externally induced poration, thus augmenting the discrimination power between perforated and intact membranes.

In contrast to fluorescence and SEM microscopy obtained within the first day-in-vitro (DIV), electrophysiological recordings have been performed after at least 4–5 DIV to give time for the cells to reach confluence and to exhibit spontaneous electrical activity.

Electrophysiological recordings with multielectrode arrays (MEA) have been performed with MEAs decorated with either short or tall nanopillars or with nanocones. The sample size considered for these experiments is indicated in Fig. 2 below the graphs. Our results depict a similar situation for the four kinds of nanostructures (Fig. 2). The spontaneous and unperturbed activity of HL-1 cells manifests in the MEA as spikes with a typical extracellular waveform.

Variations in amplitude among the signals recorded on different nanostructures is observed. However, this can be attributed to differences of the cell coupling strength. In particular, the extracellular recordings with SSP present in average a lower amplitude (panels a and i in Fig. 2), potentially due to the additional thin passivation that covers the planar electrode and the lateral sides of the short pillars, leaving only the pillars' tips exposed to the cells.

Subsequently, we perform electroporation of the cellular membrane by applying short electrical pulses through the nanostructures following previous protocols[11,23]. For all the tested geometries, this leads to the recording of intracellular action potentials, confirming that the cellular membrane is porated and that the nanostructures are in direct contact with the intracellular domain (Fig. 2). As for spontaneous extracellular recording, after electroporation we observe differences in amplitude and waveform of the intracellular action potentials among the different 3D nanostructures. This is expected due to the variations in aspect ratio and shape among SSP, STP, STC, and SP that lead to changes in the membrane cleft and, thus, in the cell/electrode coupling. In particular, the signals from nanocones preserve a larger extracellular component, probably because of the smoother profile of a nanocone compared to nanopillars that may result in a milder electroporation.

The cellular membrane reseals typically within few tens of minutes after electroporation. We observe this behavior in measurements performed with all 3D nanostructures, where the action potential shape gradually returning to a full extracellular waveform. The recovery of the pure extracellular waveform indicates that the cellular membrane can reconstruct itself around the nanostructures independently of their shape.

In very rare cases (~1.6%) at 4 DIV and using SP, we observed unperturbed activity with a partial intracellular contribution, which gave a mixed extra/intracellular waveform shape to the recorded spikes (Fig. S3B). However, in this case, the spontaneously established intracellular coupling seems to be only partial. In fact, after application of electroporation, the nanostructures strengthen their intracellular coupling and the recorded signals change shape (Fig. S3C), acquiring a longer duration as expected for intracellular action potentials. Given the higher sharpness and the smaller diameter of the sharp nanopillars (~80 nm) in

contrast to the other nanostructures, it is possible here to observe such rare occurrences of spontaneous intracellular signals. Moreover, these data highlight the possibility to advance towards spontaneous, strong and stable intracellular coupling with sharp nanopillar structures below this diameter, as already suggested in previous literature[18,23].

We performed electrophysiological experiments with engineered spiking HEK293 cells[24] in addition to the main tests with HL-1 cells. The electrical recordings of spontaneous HEK activity was recorded using hollow iridium oxide (IrOx) nanotubes[13]. In very rare cases, within the first 24 hours of culture, we have recorded intracellular action potentials from HEK cells on IrOx nanotubes without performing electroporation (Fig. S3A). These rare events suggest that spontaneous cellular membrane poration may occur during the initial hours after cell plating. However, this spontaneous penetration of the nanostructures into the cells appears to have mostly transient dynamics, with a full recovery of the membrane integrity after 3–4 DIV as confirmed by our electrophysiological recordings of HL-1 and by previous experiments[13].

To better relate cell membrane poration with the fluorescence staining shown in Figure 1, we performed also a combined experiment in which we recorded intracellular activity and stained HL-1 by creating pores by means of electroporation with SP (Fig. S4). Here, we added propidium iodide (PI) to the cell medium of HL-1 cells cultured on a MEA decorated with sharp pillars. PI is membrane-impermeant, as calcein, and stains only dead cells or cells with porated membrane[10]. By performing electroporation, we record intracellular action potentials from the cells sitting on the electrodes and, at the same time, we observe that these cells internalize PI and show red fluorescence in the nuclei (Fig. S4A). On the contrary, non-electroporated cells do not show red fluorescence, and the respective electrodes record extracellular signals (Fig. S4B). This experiment establishes a strong connection between the creation of pores in the cellular membrane and the internalization of membrane-impermeant dyes, thus supporting the results of fluorescence microscopy shown in Fig. 1.

SEM/FIB cross-sectioning

The membrane/3D nanostructure interface has been investigated in detail by observing the samples with SEM after cross-sectioning with FIB. Recent advancements in SEM/FIB microscopy of fixed cells allow clear observation of the cellular membrane profile after ultra-thin plasticization (UTP)[5,25]. In fact, it was shown that the UTP procedure does not influence the cellular morphology of the chemically fixed cells, making the observations reliable and comparable to those obtained with live cells[5]. The high resolution of the technique (approx. 5–10 nm) also allows an evaluation of the membrane's integrity and detection of possible rupture sites.

HL-1 cells have been cultured on samples with SSP, STP, STC, and SP and fixed during the approaching (4h) and spreading phases (24h). Heavy metals have been loaded into the samples to increase the SEM image contrast of the protein and lipid cellular components[26,27]. Detailed specimen preparation is described in the Experimental Procedure in supplementary information.

The results of the SEM characterization of the membrane/3D nanostructure interface are evaluated for the two culture phases and for the four nanostructures investigated in this work (Fig. 3). The images have inverted shading to highlight the cell constituents. As a first observation, we notice that the SEM image resolution and contrast are sufficient to discern clearly intracellular structures such as mitochondria and the endoplasmic reticulum. More importantly, the cellular membrane can be seen adhering to the substrates, allowing for the proper characterization of the cleft and membrane integrity.

The images show that, independent of the nanostructure shape and size, the cellular membrane tends to adhere to the substrate and along the full profile of the nano-object, including the sharp edge at the base of the nanopillars. In addition, there is no evident difference in the membrane's conformation between the approaching and the spreading phases across different geometries.

In this work, we show that cells have robust and highly flexible membranes which are able to adapt and adhere to various sharp 3D structures at the nanoscale. The confidence of our investigation stems from a thorough characterization by means of comprehensive and complementary techniques that provide information on several aspects of the biological behavior of the interface, both in physiological conditions and in a fixated state. In particular, we have observed the cell/nanostructure interface directly with SEM cross-sectional microscopy and we have evaluated the membrane integrity in real-time by means of fluorescence microscopy and electrophysiological recordings, taking into account various culture phases from a few hours after plating to 4–5 DIV. In the majority of our experiments, spontaneous cell poration has not been detected at any culture development stage. Rare events of spontaneous intracellular recordings have been obtained only with spiking HEK cells on IrOx nanotubes within the first day after plating and with HL-1 cells on sharp nanopillars after 4 DIV. Overall, these results provide important insights in the design of nanostructures' shape and size to control spontaneous intracellular access, and can help engineering novel high performance biomedical devices.

Supplementary Material

Refer to Web version on PubMed Central for supplementary material.

Acknowledgment

The research leading to these results has been partially funded by the European Research Council under the European Union's Seventh Framework Programme (FP/2007–2013)/ERC Grant Agreement no. [616213], CoG: Neuro-Plasmonics. F.S. thanks Dr. Valentina Mollo for the help with the specimen preparation for the SEM/FIB.

References

(1). Xie X; Xu AM; Leal-Ortiz S; Cao Y; Garner CC; Melosh NA Nanostraw-Electroporation System for Highly Efficient Intracellular Delivery and Transfection. ACS Nano 2013, 7 (5), 4351–4358. [PubMed: 23597131]

(2). Tian B; Cohen-Karni T; Qing Q; Duan X; Xie P; Lieber CM Three-Dimensional, Flexible Nanoscale Field-Effect Transistors as Localized Bioprobes. Science 2010, 329, 830–834. [PubMed: 20705858]

(3). Gartia MR; Hsiao A; Sivaguru M; Chen Y; Logan Liu G Enhanced 3D Fluorescence Live Cell Imaging on Nanoplasmonic Substrate. Nanotechnology 2011, 22 (36).

(4). Zhao W; Hanson L; Lou H-Y; Akamatsu M; Chowdary PD; Santoro F; Marks JR; Grassart A; Drubin DG; Cui Y; et al. Nanoscale Manipulation of Membrane Curvature for Probing Endocytosis in Live Cells. Nat. Nanotechnol 2017, 12 (8), 750–756. [PubMed: 28581510]

(5). Santoro F; Zhao W; Joubert L-M; Duan L; Schnitker J; van de Burgt Y; Lou H-Y; Liu B; Salleo A; Cui L; et al. Revealing the Cell-Material Interface with Nanometer Resolution by Focused Ion Beam/Scanning Electron Microscopy. ACS Nano 2017, 11 (8), 8320–8328. [PubMed: 28682058]

(6). Santoro F; Dasgupta S; Schnitker J; Auth T; Neumann E; Panaitov G; Gompper G; Offenhäusser A Interfacing Electrogenic Cells with 3D Nanoelectrodes: Position, Shape, and Size Matter. ACS Nano 2014, 8 (7), 6713–6723. [PubMed: 24963873]

(7). Xie C; Lin Z; Hanson L; Cui Y; Cui B Intracellular Recording of Action Potentials by Nanopillar Electroporation. Nat. Nanotechnol 2012, 7, 185–190. [PubMed: 22327876]

(8). Spira ME; Hai A Multi-Electrode Array Technologies for Neuroscience and Cardiology. Nat. Nanotechnol 2013, 8, 83–94. [PubMed: 23380931]

(9). Dipalo M; Amin H; Lovato L; Moia F; Caprettini V; Messina GC; Tantussi F; Berdondini L; De Angelis F; Angelis F. De. Intracellular and Extracellular Recording of Spontaneous Action Potentials in Mammalian Neurons and Cardiac Cells with 3D Plasmonic Nanoelectrodes. Nano Lett. 2017, 17 (6), 3932–3939. [PubMed: 28534411]

(10). Messina GC; Dipalo M; La Rocca R; Zilio P; Caprettini V; Proietti Zaccaria R; Toma A; Tantussi F; Berdondini L; De Angelis F Spatially, Temporally, and Quantitatively Controlled Delivery of Broad Range of Molecules into Selected Cells through Plasmonic Nanotubes. Adv. Mater 2015, 27, 7145–7149. [PubMed: 26445223]

(11). Caprettini V; Cerea A; Melle G; Lovato L; Capozza R; Huang J-A; Tantussi F; Dipalo M; De Angelis F Soft Electroporation for Delivering Molecules into Tightly Adherent Mammalian Cells through 3D Hollow Nanoelectrodes. Sci. Rep 2017, 7 (1).

(12). Cao Y; Hjort M; Chen H; Birey F; Leal-Ortiz SA; Han CM; Santiago JG; Pa§ca, S. P.; Wu, J. C.; Melosh, N. A. Nondestructive Nanostraw Intracellular Sampling for Longitudinal Cell Monitoring. Proc. Natl. Acad. Sci 2017, 114 (10), E1866–E1874. [PubMed: 28223521]

(13). Lin ZC; Xie C; Osakada Y; Cui Y; Cui B Iridium Oxide Nanotube Electrodes for Sensitive and Prolonged Intracellular Measurement of Action Potentials. Nat. Commun 2014, 5, 3206. [PubMed: 24487777]

(14). Lin ZC; McGuire AF; Burridge PW; Matsa E; Lou H-Y; Wu JC; Cui B Accurate Nanoelectrode Recording of Human Pluripotent Stem Cell-Derived Cardiomyocytes for Assaying Drugs and Modeling Disease. Microsystems Nanoeng. 2017, 3, 16080.

(15). Vandersarl JJ; Xu AM; Melosh NA Nanostraws for Direct Fluidic Intracellular Access. Nano Lett. 2012, 12 (8), 3881–3886. [PubMed: 22166016]

(16). Kim W; Ng JK; Kunitake ME; Conklin BR; Yang P Interfacing Silicon Nanowires with Mammalian Cells. J. Am. Chem. Soc 2007, 129 (23), 7228–7229. [PubMed: 17516647]

(17). Chiappini C; De Rosa E; Martinez JO; Liu X; Steele J; Stevens MM; Tasciotti E Biodegradable Silicon Nanoneedles Delivering Nucleic Acids Intracellularly Induce Localized in Vivo Neovascularization. Nat. Mater 2015, 14 (5), 532–539. [PubMed: 25822693]

(18). Xu AM; Aalipour A; Leal-Ortiz S; Mekhdjian AH; Xie X; Dunn AR; Garner CC; Melosh NA Quantification of Nanowire Penetration into Living Cells. Nat. Commun 2014, 5, 3613. [PubMed: 24710350]

(19). Xie X; Aalipour A; Gupta SV; Melosh NA Determining the Time Window for Dynamic Nanowire Cell Penetration Processes. ACS Nano 2015, 9 (12), 11667–11677. [PubMed: 26554425]

(20). Kono K; Igawa T; Takagishi T Cytoplasmic Delivery of Calcein Mediated by Liposomes Modified with a PH-Sensitive Poly(Ethylene Glycol) Derivative. Biochim. Biophys. Acta - Biomembr. 1997, 1325 (2), 143–154.

(21). Alemayehu A Gorfe; Hocker HJ Membrane Targeting: Methods. eLS 2012, 1.

(22). Hai A; Shappir J; Spira ME In-Cell Recordings by Extracellular Microelectrodes. Nat. Methods 2010, 7 (3), 200–202. [PubMed: 20118930]

(23). Duan X; Gao R; Xie P; Cohen-Karni T; Qing Q; Choe HS; Tian B; Jiang X; Lieber CM Intracellular Recordings of Action Potentials by an Extracellular Nanoscale Field-Effect Transistor. Nat. Nanotechnol 2012, 7 (3), 174–179.

(24). Park J; Werley CA; Venkatachalam V; Kralj JM; Dib-Hajj SD; Waxman SG; Cohen AE Screening Fluorescent Voltage Indicators with Spontaneously Spiking HEK Cells. PLoS One 2013, 8 (12).

(25). Belu A; Schnitker J; Bertazzo S; Neumann E; Mayer D; OffenhÄusser A; Santoro F Ultra-Thin Resin Embedding Method for Scanning Electron Microscopy of Individual Cells on High and Low Aspect Ratio 3D Nanostructures. J. Microsc 2016, 263 (1), 78–86. [PubMed: 26820619]

(26). Tapia JC; Kasthuri N; Hayworth KJ; Schalek R; Lichtman JW; Smith SJ; Buchanan J High-Contrast En Bloc Staining of Neuronal Tissue for Field Emission Scanning Electron Microscopy. Nat. Protoc 2012, 7 (2), 193–206. [PubMed: 22240582]

(27). Bushby AJ; P'Ng KMY; Young RD; Pinali C; Knupp C; Quantock AJ Imaging Three-Dimensional Tissue Architectures by Focused Ion Beam Scanning Electron Microscopy. Nat. Protoc 2011, 6 (6), 845–858. [PubMed: 21637203]

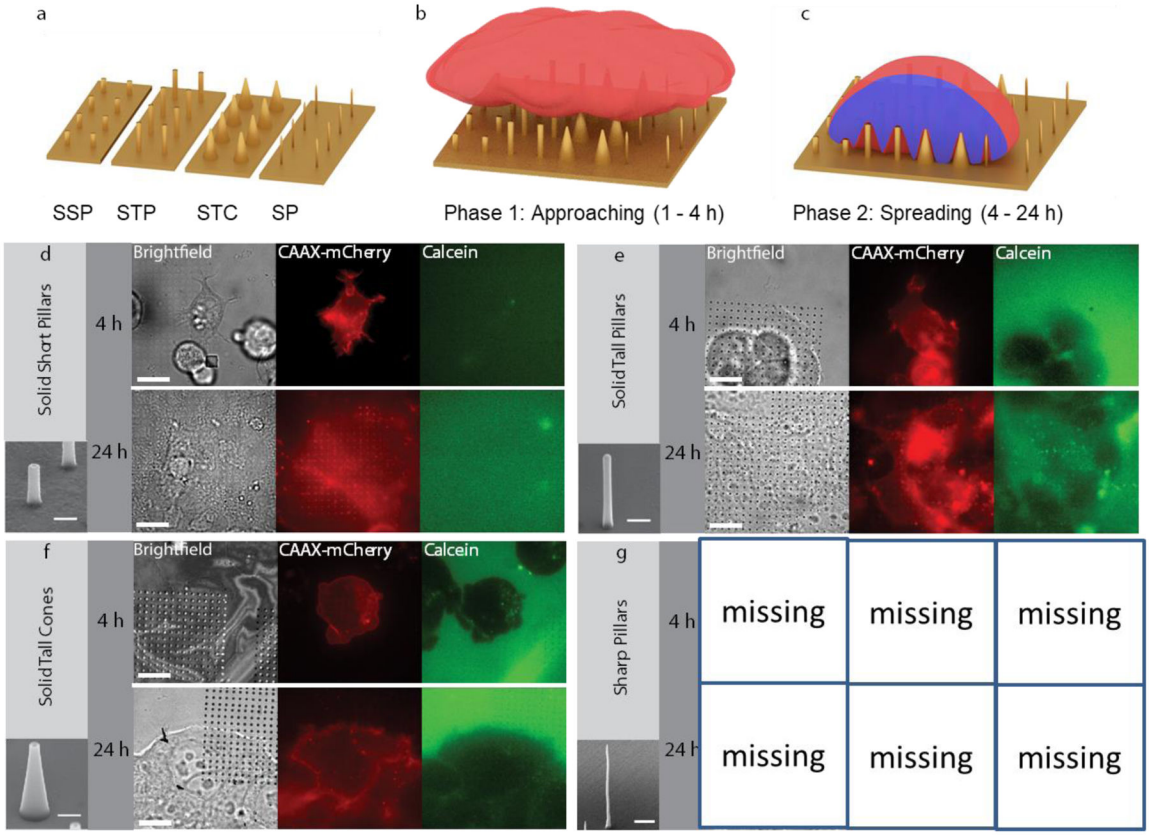

Figure 1.

Schematic and fluorescence imaging of penetration. a) 3D sketch of the main nanostructures. b) Sketch of a cell approaching the nanostructures (< 4 h incubation). c) Sketch of a cell in adhesion on the different 3D nanostructures (< 24 h incubation). Images of Caax-mCherry-transfected HEK cells on d) SSPs, e) STPs, f) STCs, and g) SP after delivery of calcein. Brightfield images show where nanostructures are located with respect to the HEK cells. Cells on all nanostructures do not show uptake of membrane-impermeant calcein (green channel). Insets show SEM of the different structures. Scale bars 15 μm. Inset scale bars 500 nm. Enlarged versions of these images are available in supporting information (Fig. S13 to S15).

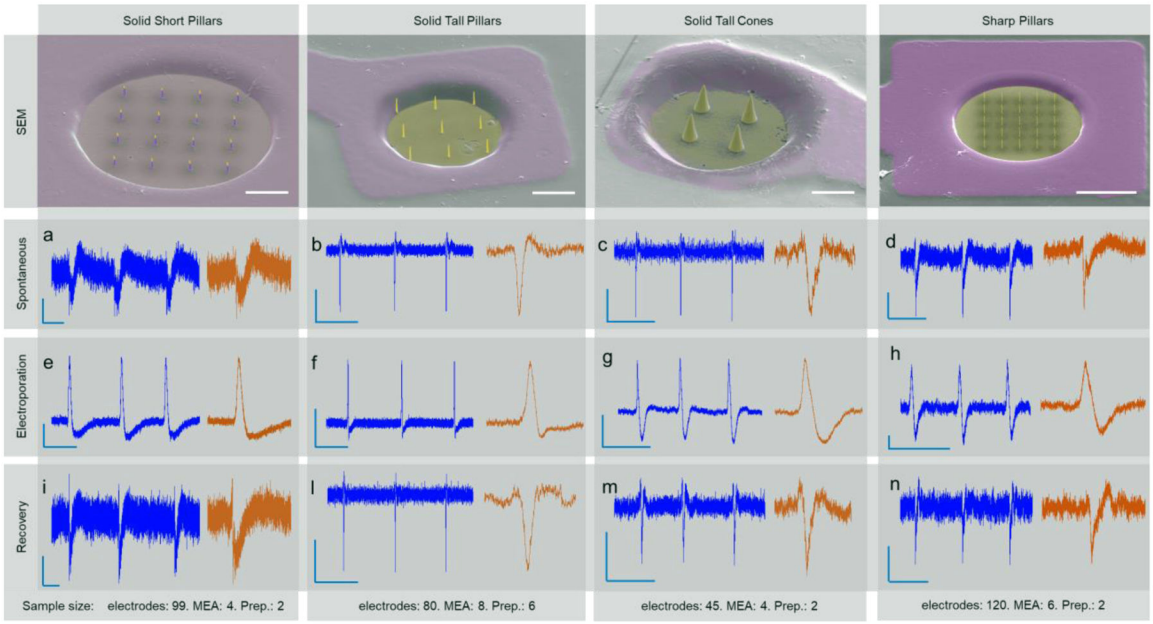

Figure 2.

SEM microscopy and electrophysiology with MEA electrodes with SSPs, STPs, STCs, and SPs. a-e-i) HL-1 action potentials recorded on SSP, respectively spontaneous activity, after electroporation and after recovery (Scale bars -- a, e: 20uV, 1s. i: 50uV, 1s). b-f-i) HL-1 action potentials recorded on STP, respectively spontaneous activity, after electroporation, and after recovery (Scale bars -- b, f: 0.1 mV, 0.5 s. i: 0.4 mV, 0.5 s). c-g-m) HL-1 action potentials recorded on STP, respectively spontaneous activity, after electroporation, and after recovery (Scale bars --c-g-m: 0.1 mV, 1 s.). d-h-n) HL-1 action potentials recorded on SP, respectively spontaneous activity, after electroporation, and after recovery (Scale bars -- d-h-n: 0.05 mV, 1 s.). Below each panel, the sample size for each nanostructure shape is indicated in terms of number of electrodes (considering only those recording activity), MEAs, and cell preparations.

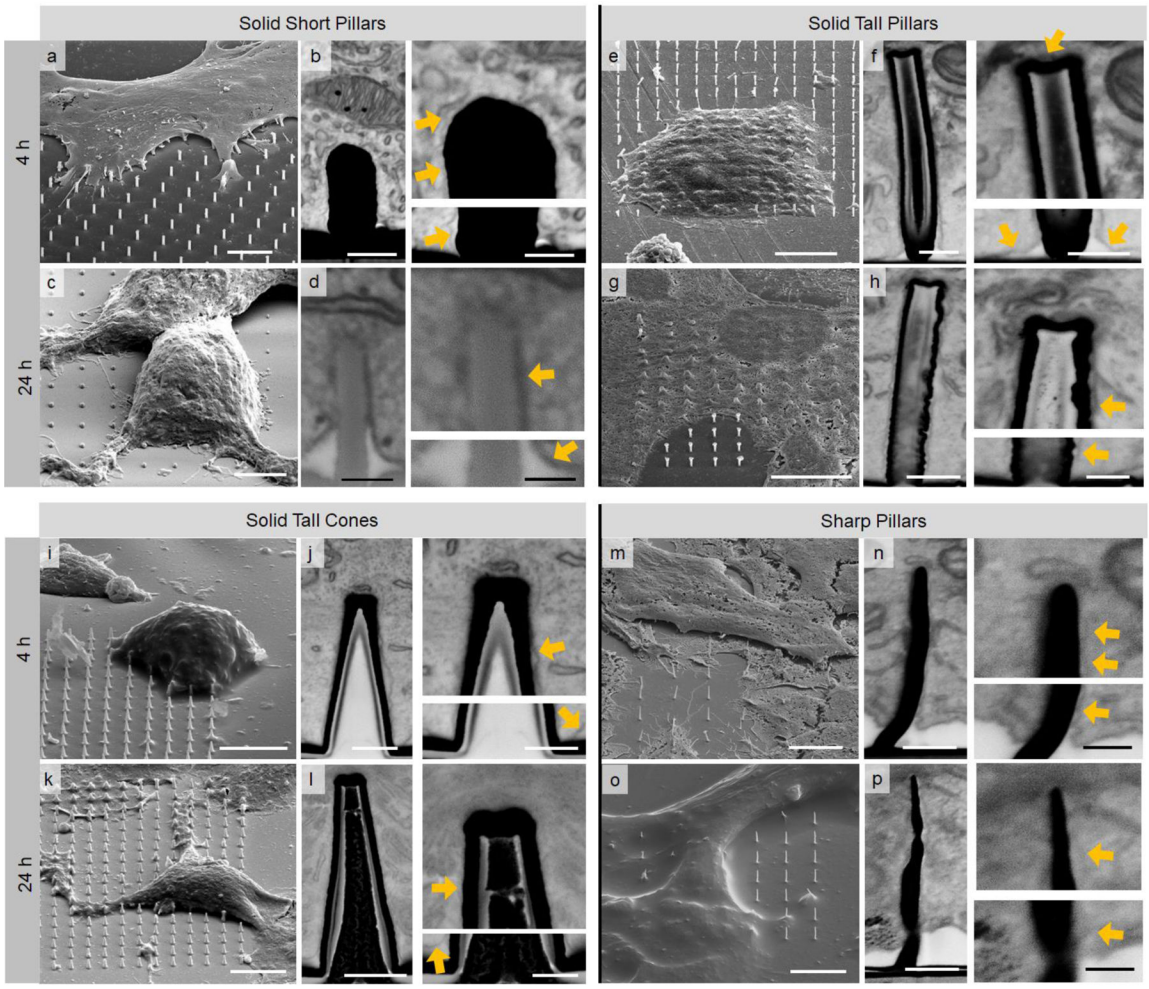

Figure 3.

SEM whole and cross-sectional images of HL-1 cultured and UTP-fixed on SSP, STP, STC, and SP. (Scale bars--a: 5 μm; b: left = 500 nm, right = 300 nm; c: 5 μm; d: left = 200 nm, right = 300 nm; e: 10 μm; f: left = 300 nm, right = 300 nm; g: 10 μm; h: left = 400 nm, right = 200 nm; i: 10 μm; j: left = 500 nm, right = 400 nm; k: 10 μm; l: left = 500 nm, right = 250 nm; m: 5 μm; n: left = 200 nm, right = 100 nm; o: 6 μm; p: left = 200 nm, right = 100 nm). Yellow arrows indicate the intact cell membrane in adhesion with the 3D nanostructures. Larger versions of all the SEM images are available in supporting information (Fig. S5 to Fig. S12).